ZONAL ANALYSIS OF TWO HIGH-SPEED INLETS

A. D. Dilley, G. F. Switzer, and W. M. Eppard *
Analytical Services and Materials, Inc.
Hampton, VA 23666

ABSTRACT

Using a zonal technique, thin-layer Navier-Stokes solutions for two high-speed inlet geometries are presented and compared with experimental data. The first configuration consists of a three-dimensional inlet preceded by a sharp flat plate. Results with two different grids demonstrate the importance of adequate grid refinement in high-speed internal flow computations. The fine grid solution has reasonably good agreement with experimental heat transfer and pressure values inside the inlet. The other configuration consists of a three-dimensional inlet mounted on a research hypersonic forebody. Numerical results for this configuration have good agreement with experimental pressure data along the forebody, but not inside the inlet. A more refined grid calculation is currently being done to better predict the flowfield in the inlet.

INTRODUCTION

The design and analysis of hypersonic air-breathing vehicles, such as the National Aerospace Plane (NASP), requires accurate prediction of propulsion system performance. Computational Fluid Dynamics (CFD) is being challenged to play a major role in the analysis of hypersonic air-breathing vehicles, because of a lack of ground test facilities to simulate the entire hypersonic flight regime and design time constraints. Existing computational tools are therefore being refined and calibrated using existing wind tunnel data, and wind tunnel tests are planned to enlarge the available hypersonic database. Comparisons of this wind tunnel data with CFD predictions will build confidence in the ability of CFD to provide accurate performance predictions for hypersonic air-breathing vehicles.

The CFD analysis of a hypersonic air-breathing propulsion system requires analysis of the entire vehicle, because the forebody externally compresses the flow ahead of the inlet and the afterbody externally expands the flow from the nozzle. Therefore a nose-to-tail CFD capability is necessary for realistic CFD analyses of hypersonic air-breathing vehicles. In an effort to develop a nose-to-tail capability, a zonal technique has been implemented in an upwind, finite volume thin-layer Navier-Stokes solver, CFL3D (reference 1). Results from the CFL3D code have previously been compared with experimental data for hypersonic laminar and turbulent forebody flows (reference 2), turbulent flow in a two-dimensional hypersonic inlet (references 3 and 4) and hypersonic laminar flows with inviscid/viscous interaction (reference 5). The zonal or patched grid approach was used by Thomas *et al* (reference 4) in the analysis of turbulent flow in several two-dimensional hypersonic inlets. The zonal approach allows regions of a complex flowfield to have different grid topologies while computing the entire flowfield with the same CFD code. Zonal grids may also lead to more efficient solution procedures by tailoring the grids to the local geometry and flow physics, and this can eliminate wasted points and inefficient grid topologies.

A recent joint government/industry code validation effort (Generic Option #2) included an extensive ground test program. The data from these ground tests are now available in a final report (reference 6).

*This work was supported by the Computational Methods Branch, Fluid Mechanics Division of NASA Langley Research Center under contract NAS1-18599.

Several inlet models were tested as part of this program, and data from the inlet tests have been used in a code validation effort using the zonal version of CFL3D. The previous code validation of CFL3D (references 3 and 4) involved two-dimensional inlet geometries. The inlets tested as part of the Generic Option #2 program have three-dimensional geometries and are mounted on representative forebodies. Numerical solutions for two of these inlets are compared below with experimental data to calibrate the forebody/inlet zonal approach implemented in CFL3D.

MODEL GEOMETRY AND COMPUTATIONAL GRIDS

Several inlet models were tested in the Calspan 96 Inch Shock Tunnel as part of the Generic Option #2 program. The objective of these tests was to obtain detailed forebody and internal flowfield measurements on NASP-like geometries at NASP-like freestream conditions. The data from the tests was intended to provide a database for validating CFD codes at hypersonic flow conditions. Numerical solutions for two of these inlets, the 2-D Internal Flow Model and the 3-D Forebody/Inlet Integration Model, are compared with data from the final report (reference 6) for the purpose of validating the zonal forebody/inlet version of CFL3D. The geometry definitions of these two configurations were based upon data from the model designers and the final report. All computational grids were generated using a modified transfinite interpolation (algebraic) grid generation method (reference 7).

The 2-D Internal Flow Model is shown in figure 1. This model consists of an inlet preceded by a flat plate. The geometry used in the present study has a sharp leading edge, however a blunt leading edge model was also tested at Calspan. The inlet was designed to have the bow-shock impinge on the cowl-lip at a freestream Mach number of 12. The inlet sidewalls have a sweep of 45 degrees, but no sidewall compression. In this analysis, the cowl leading edge is also sharp. The inlet was designed to be tested at several contraction ratios; the configuration used in this study has a contraction ratio of five.

The grid topology for the 2-D Internal Flow Model is shown in figure 2. The grid for this model consists of five blocks/zones with half the inlet gridded because of symmetry considerations. A two-dimensional boundary layer solution is stored in the first block to initialize the inlet calculation. A one-to-one patch interface boundary condition between blocks one and two communicates the boundary layer solution to the inlet. Block two starts ahead of the 8 degree ramp to capture any ramp-induced separation bubbles. Block three has grid stretching from the sidewall and is patched into block two. The sidewall sweep is modelled in block three by a "jagged" wall/no wall boundary condition allowing the cross-sectional grid to remain in a vertical plane, thus simplifying the grid generation. The internal portion of the inlet consists of the last two blocks. In CFL3D, turbulent flow from two opposing surfaces, such as a cowl and a ramp, cannot be calculated with one computational block, but requires upper and lower computational blocks as shown in figure 2.

The 3-D Forebody/Inlet Integration Model is shown in figure 3. This model has a blunt nosetip with a nose radius of 0.27 inches, followed by a 3 degree forebody. A system of lower surface compression ramps (7 degrees and 11 degrees) precedes the inlet. The inlet module was designed to have the bow-shock impinge on the cowl-lip at a freestream Mach number of 16.5. Also, the inlet module has no sidewall sweep and no sidewall compression. The inlet was designed to test several contraction ratios; the configuration used in this study has a contraction ratio of two.

The grid topology for the 3-D Forebody/Inlet Integration Model is shown in figure 4. The grid consists of three computational zones: the blunt nose, the forebody and the inlet. As before, half the configuration is gridded because of symmetry considerations. The blunt nose zone, the forebody zone and the location of the inlet at the outflow plane of the forebody are indicated in figure 4. The inlet zone (not shown) consists of two internal blocks similar to the 2-D Internal Flow Model. Patch interface boundary conditions connect the zones, allowing information to pass from one zone to the adjacent zone.

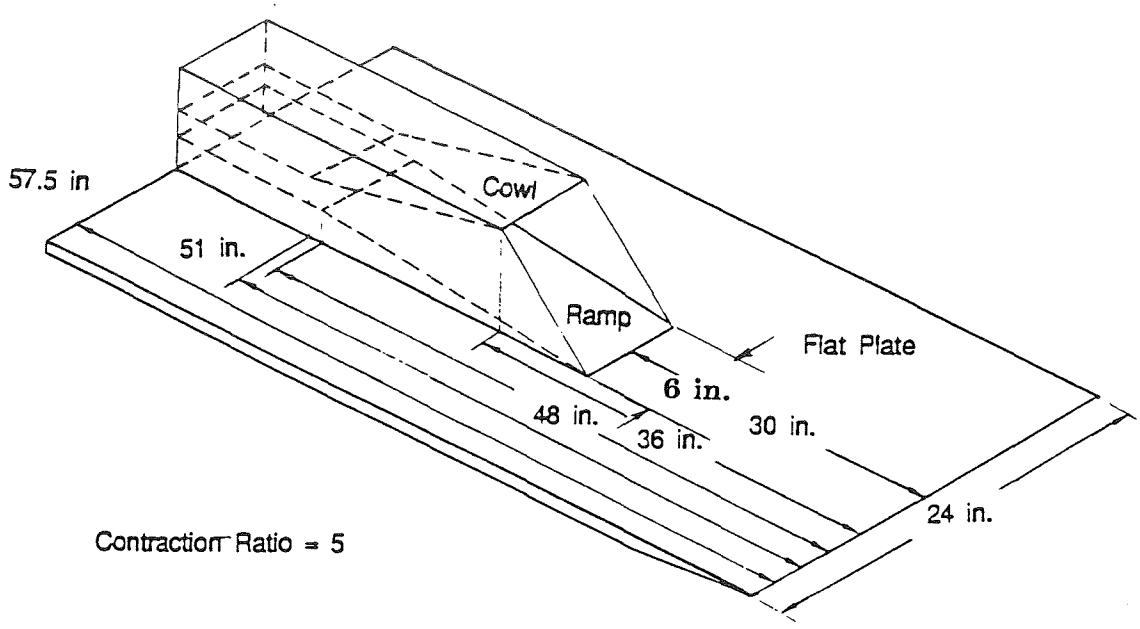

Figure 1. Schematic of 2-D Internal Flow Model.

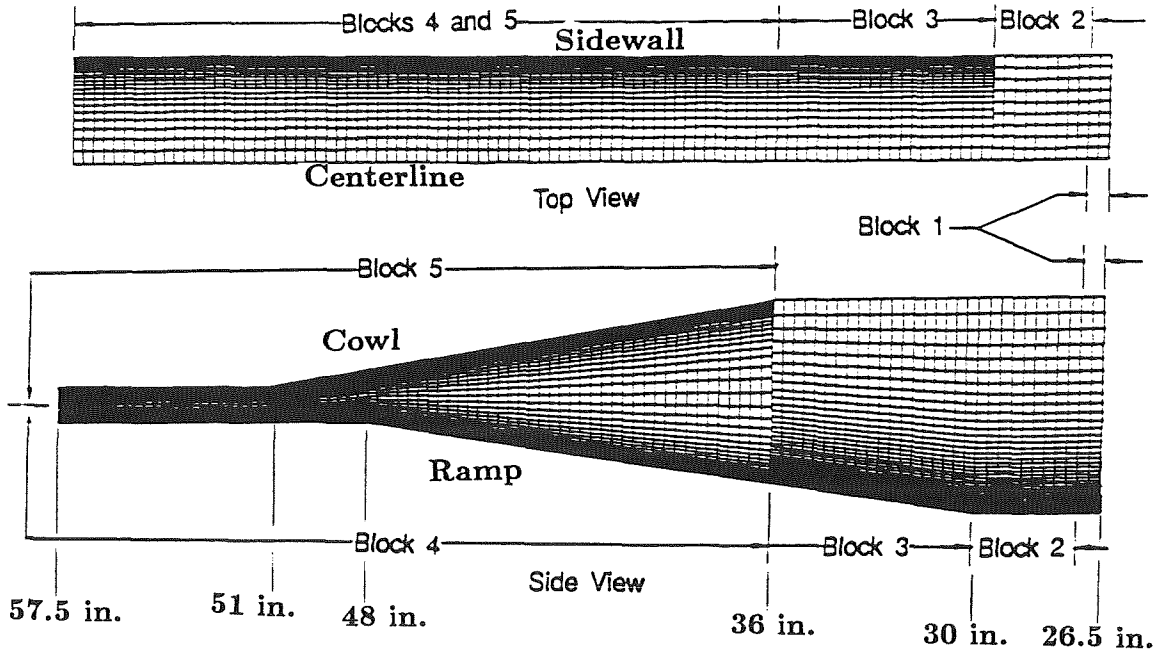

Figure 2. 2-D Internal Flow Model grid topology.

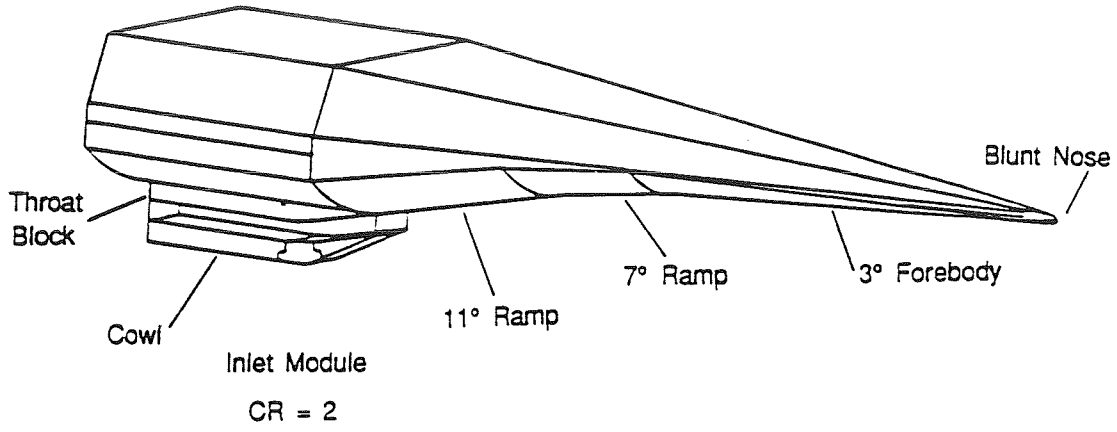

Figure 3. Schematic of 3-D Forebody/Inlet Integration Model.

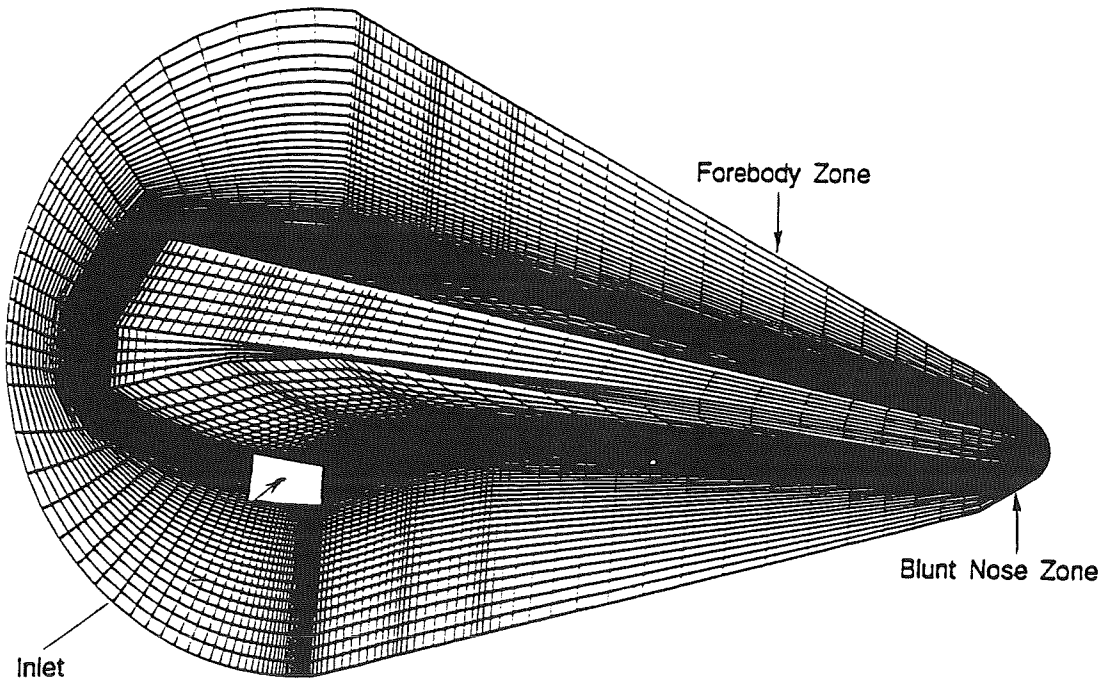

Figure 4. 3-D Forebody/Inlet Integration Model grid topology.

DISCUSSION OF RESULTS

The Generic Option #2 program has provided a large amount of test data on NASP-like geometries at NASP-like freestream conditions. This data is currently being used in validating CFD codes at hypersonic flow conditions. Numerical solutions for two inlet geometries tested at Calspan are compared with test data as part of a code validation effort at the NASA Langley Research Center. In analyzing these comparisons, the term, y^+, will be used. Here, y^+ is defined as:

$$y^+ = \Delta y \frac{\left(\frac{\tau_w}{\rho}\right)^{\frac{1}{2}}}{\nu} \tag{1}$$

where Δy is the normal distance of the first cell center off the body, ρ is the density, τ_w is the wall shear stress and ν is the kinematic viscosity. Generally, smaller values of y^+ indicate a finer grid near the body. The numerical solutions presented below are not considered to be grid converged, but are of use in assessing the forebody/inlet capabilities of the zonal version of CFL3D. In one case, a grid refinement calculation is underway and results may be available for the oral presentation. Both inlet calculations used a Baldwin-Lomax turbulence model (reference 8) to model turbulent flow regions.

The 2-D Internal Flow Model consists of an inlet module preceded by a flat plate. The model was designed to have high contraction ratio, internal flow passages which admitted instrumentation to make off-body flow field measurements. The model instrumentation was concentrated in the inlet module and included heat transfer and pressure gauges, along with several pitot pressure rake measurement stations. The heat transfer and pressure gauges were located along the centerline of the inlet and 0.35 inches from the sidewalls.

Results for the 2-D Internal Flow Model are shown in figures 5 through 10. The freestream conditions for this case were: a zero degree angle of attack, a Mach number of 12.26 and a Reynolds number of 1.049 million per foot. A two-dimensional laminar boundary layer solution provided the inflow boundary condition. A symmetry-plane boundary condition was imposed at one spanwise boundary and a "jagged" wall/no wall boundary condition at the other spanwise boundary. A fixed wall temperature was imposed on all surfaces. Based on the CFD analysis in the final report (reference 6), linear transition to turbulence on the ramp was initiated at the start of the ramp, and the flow was fully turbulent halfway up the ramp. On the cowl, following a two inch transition region, the flow was fully turbulent after the ramp shock had impinged on the cowl surface. The sidewall was treated as laminar throughout the inlet module. There was no special modelling of the corner interaction between the laminar sidewall and the turbulent cowl/ramp.

Numerical solutions were obtained on two different grids. The coarse grid consisted of five blocks (see figure 2) with 10x75x3 in block one, 10x75x10 in block two, 30x75x20 in block three, 30x38x72 in block four and 30x38x72 in block five. The grid specification gives the number of spanwise points, the number of normal points and the number of axial points. The fine grid was intended to improve the results in the internal portion of the inlet. Therefore, only blocks four and five were refined with 29x49x73 points each. The fine grid reduced the maximum y^+ by a factor of 10.

Qualitative features of the flow are shown in figures 5 and 6. In figure 5, total Mach number contours are plotted at several cross-sections. The effect of the "jagged" wall/no wall boundary condition can be seen in the boundary layer development on the sidewall. In figure 6, total Mach number contours are plotted along the symmetry plane. Separation occurs at the following locations: (1) ahead of the ramp, (2) on the cowl where the ramp shock impinges on the cowl surface and (3) on the ramp where the flow expands over the ramp shoulder. Although not shown, the fine grid solution has larger separation regions than the coarse grid solution. These results contrast with the laminar results of Reddy *et al* (reference 9). That laminar calculation predicted attached flow throughout the inlet. The Mach wave from the strong interaction at the sharp leading edge of the flat plate is evident and impinges on the cowl at approximately 42 inches from the

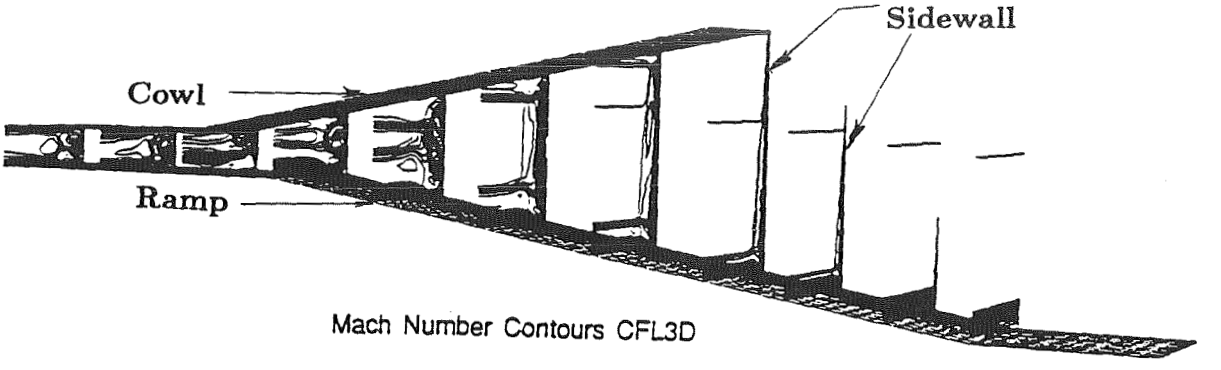

Figure 5. Cross-sectional Mach numbers inside inlet - 2-D Model.

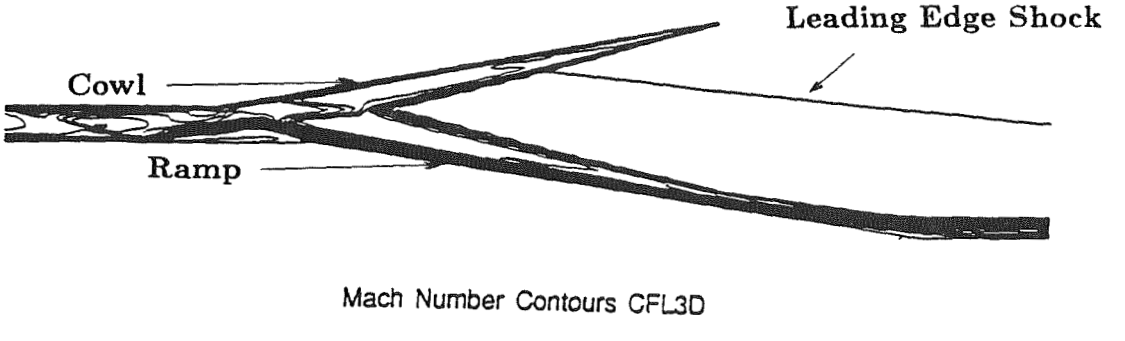

Figure 6. Symmetry plane Mach numbers inside inlet - 2-D Model.

flat-plate leading edge. The coalesced ramp and cowl shock reflect on the ramp surface and the cowl surface before exiting the inlet.

Comparisons of computed surface pressure and experimental pressure data are shown in figures 7 and 8. The heat transfer comparisons are shown in figures 9 and 10. The computed centerline values match the experimental data reasonably well. The fine grid solution has better agreement with the experimental peak heat transfer and pressure, especially on the ramp centerline. The side plane comparisons exhibit similar trends. The fine grid solution has a sharper resolution of internal shocks and their impingement on the ramp and cowl surfaces. The sharper resolution of internal shocks results in more accurate predictions of the peak values of heat transfer and pressure as shown in these figures. The coarse grid solution has a maximum y^+ of approximately 8; whereas the fine grid solution has a maximum y^+ of approximately 0.75 . The improvement in y^+ also results in better heat transfer predictions. Overall, the computed flow features generally match the experiment well.

The 3-D Forebody/Inlet Integration Model consists of a blunt nose forebody with a system of lower surface compression ramps preceding the inlet. The model was designed to study the surface and off-body flowfield characteristics associated with the external/internal contraction regions of an integrated inlet geometry. The model instrumentation included heat transfer and pressure gauges distributed on the lower forebody surface and inside the inlet module, along with several pitot pressure rake measurement stations. Heat transfer and pressure gauges were located on the forebody centerline and on several off-centerline forebody rays. On the inlet cowl and throat block, heat transfer and pressure gauges were located on the centerline and 0.35 inches from the inlet sidewall. The throat block is the extension of the lower forebody surface into the inlet module.

Results for the 3-D Forebody/Inlet Integration Model are shown in figures 11 through 15. The freestream conditions were: a zero degree angle of attack, a Mach number of 11.31 and a Reynolds number of 9.893 million per foot. These conditions correspond to the "undersped condition" given in the final report (reference 6). The blunt nose region was laminar, and transition to turbulence occurred several inches downstream of the blunt nose. Based on the final report (reference 6), the flow was fully turbulent by fuselage station 6, the first heat transfer gauge on the forebody. The flow in the inlet module was treated as fully turbulent from all surfaces, including the sidewall. This was done by using the two wall/one corner turbulence model in CFL3D and two internal computational blocks. The corner modelling allows turbulent flow from a sidewall to interact with turbulent flow from a cowl or a ramp. Symmetry-plane boundary conditions were imposed at the top and bottom centerlines of the forebody and the centerline of the inlet module. The inlet module had no sidewall sweep, therefore a "jagged" wall/no wall boundary condition was not required. A fixed wall temperature was imposed on all forebody and inlet surfaces.

The grid consisted of three computational zones with 41x65x25 on the blunt nose, 65x65x55 on the forebody and 45x65x100 in the inlet. The grid specification gives the number of circumferential points, the number of normal points and the number of axial points. The solution on this grid has a maximum y^+ of approximately 5. To reduce the maximum y^+, a finer grid is being used in a new calculation for this configuration. However, results from that calculation were not available for inclusion in this paper.

Pressure contours in the symmetry plane, in the outflow plane and on the bottom surface of the forebody are shown in figure 11. The bow shock and both ramp shocks are clearly visible in these contours. In figure 12, computed forebody pressures are compared with experimental data along the centerline and along a ray off the centerline. The agreement in this case is good. The forebody heat transfer comparisons (not shown) are poor. Contours of total Mach number at various cross-sections inside the inlet are shown in figure 13. The flow is from left to right. A large buildup of the boundary layer develops on the lower symmetry plane of the forebody and is evident partially into the inlet. Figures 14 and 15 show comparisons of computed pressures with experimental data on the cowl and the throat block of the inlet. The agreement here is not as good as on the forebody. A more refined grid calculation is currently underway. The more refined grid solution is expected to give better resolution of internal shocks, and therefore improve the pressure comparisons in the inlet and provide reasonable heat transfer comparisons. Results from the refined grid calculation may be available for the oral presentation.

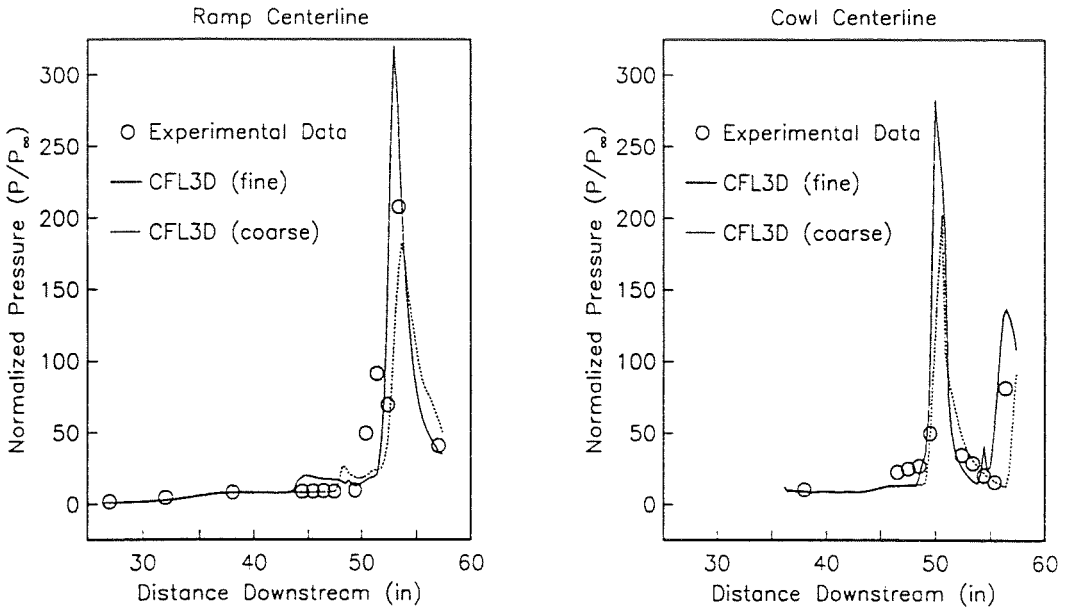

Figure 7. Pressure comparisons between CFL3D and experiment - 2-D Model, ramp centerline and cowl centerline.

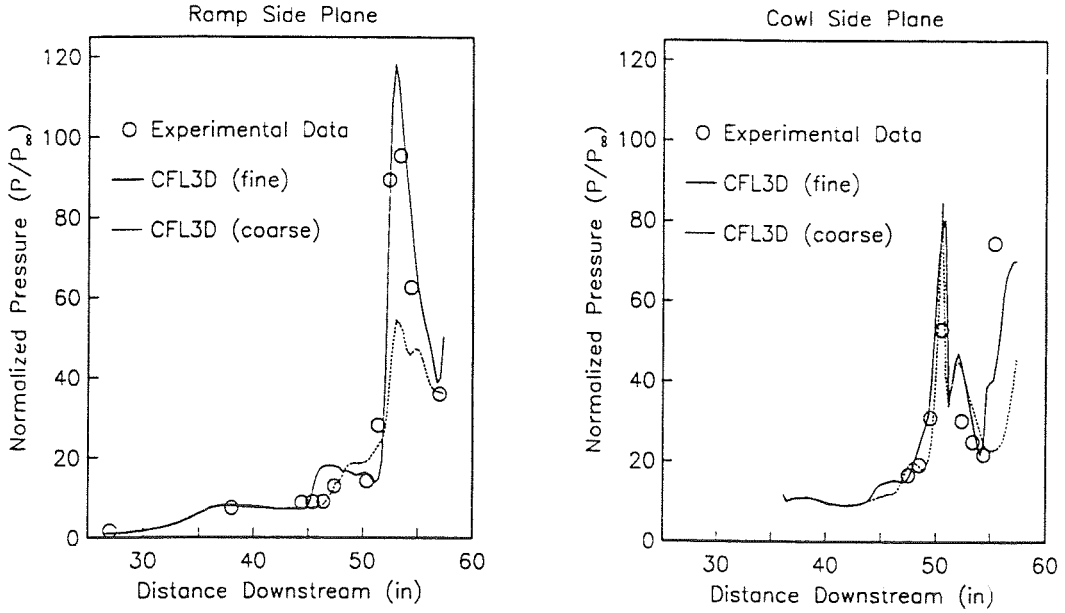

Figure 8. Pressure comparisons between CFL3D and experiment - 2-D Model, ramp side plane and cowl side plane.

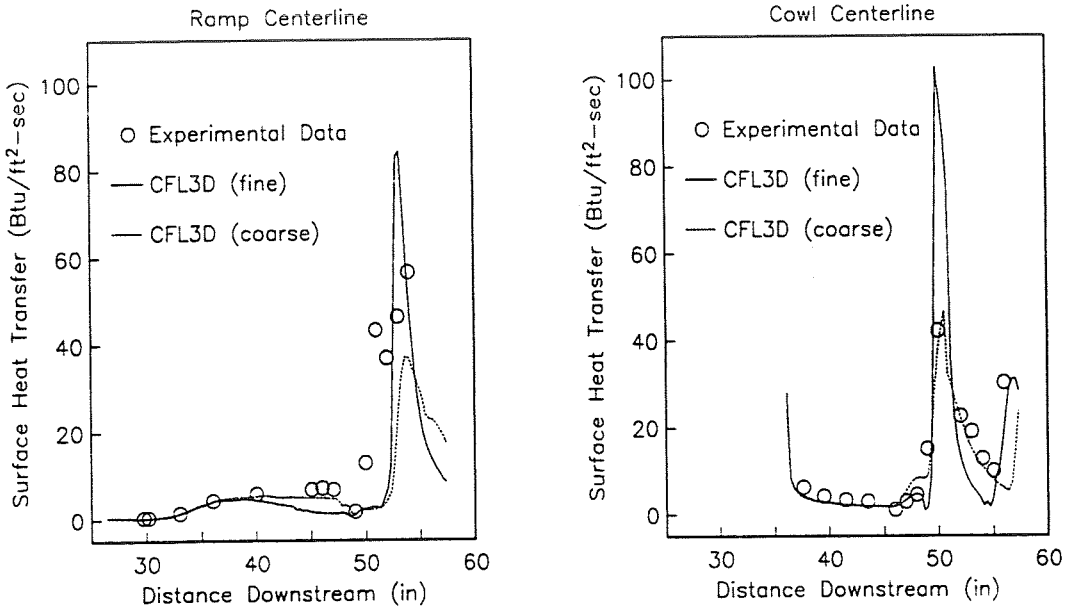

Figure 9. Heat transfer comparisons between CFL3D and experiment - 2-D Model, ramp centerline and cowl centerline.

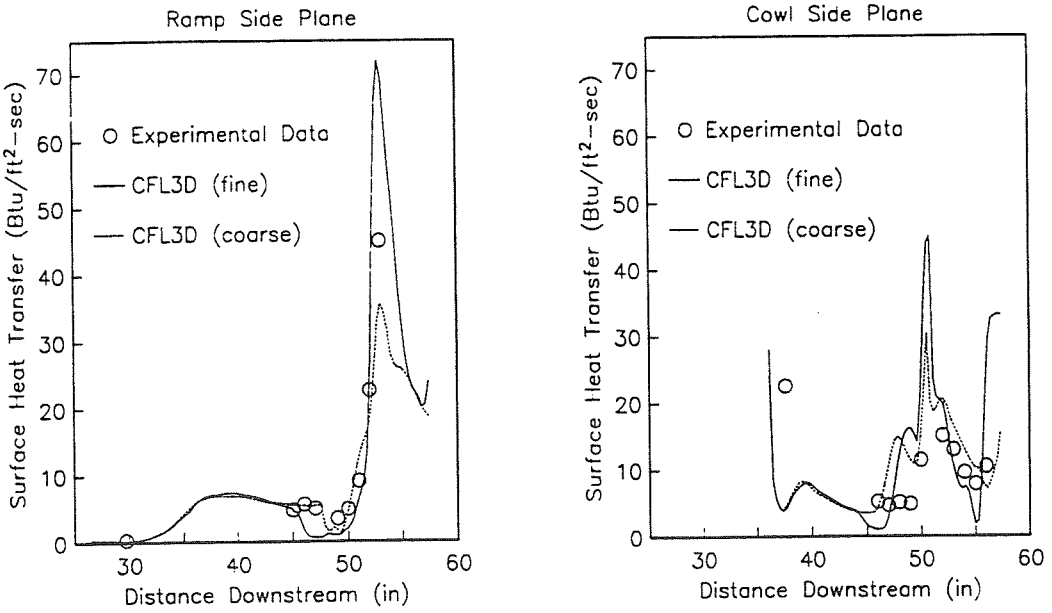

Figure 10. Heat transfer comparisons between CFL3D and experiment - 2-D Model, ramp side plane and cowl side plane.

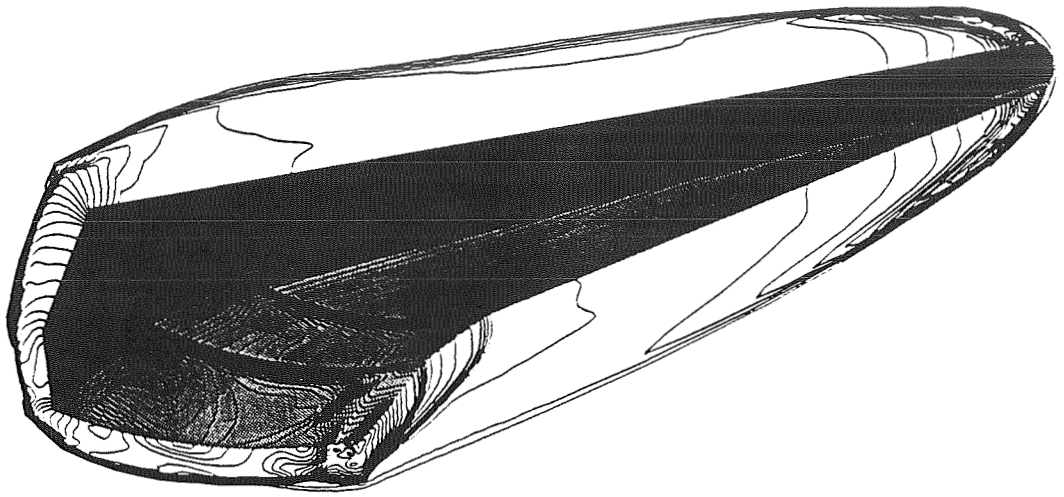

Figure 11. Pressure contours - 3-D Model, symmetry plane, outflow plane, and windward surface.

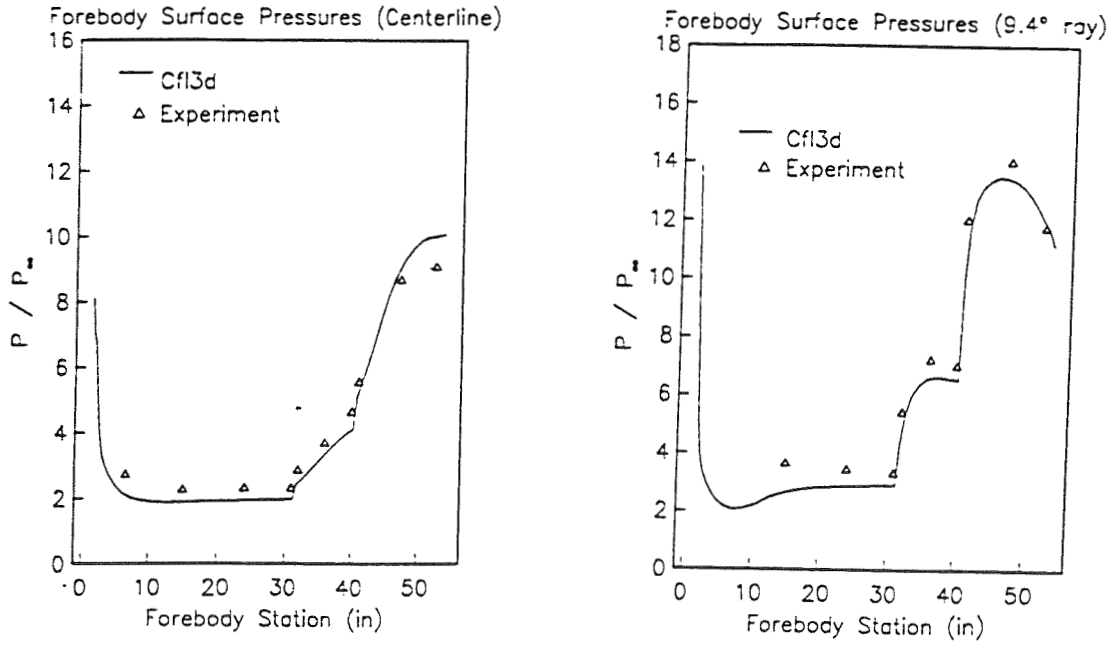

Figure 12. Pressure comparisons between CFL3D and experiment - 3-D Model, lower surface centerline and off-centerline.

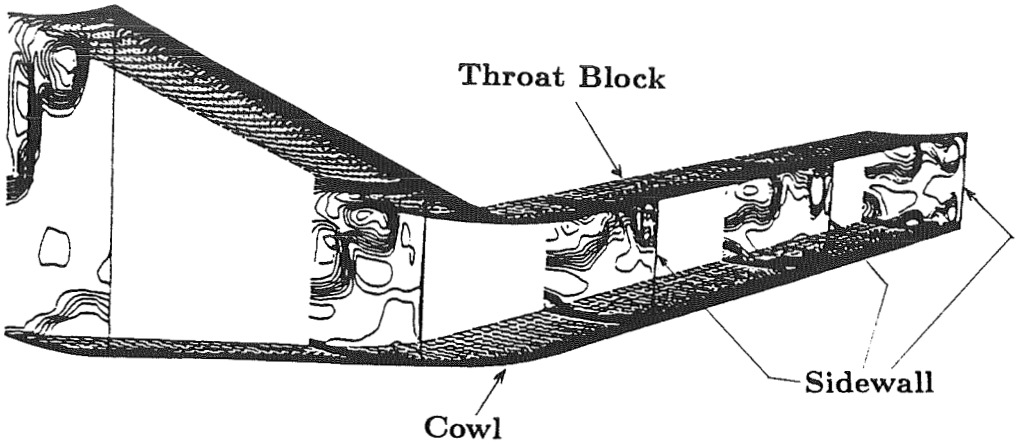

Figure 13. Cross-sectional Mach numbers inside inlet - 3-D Model.

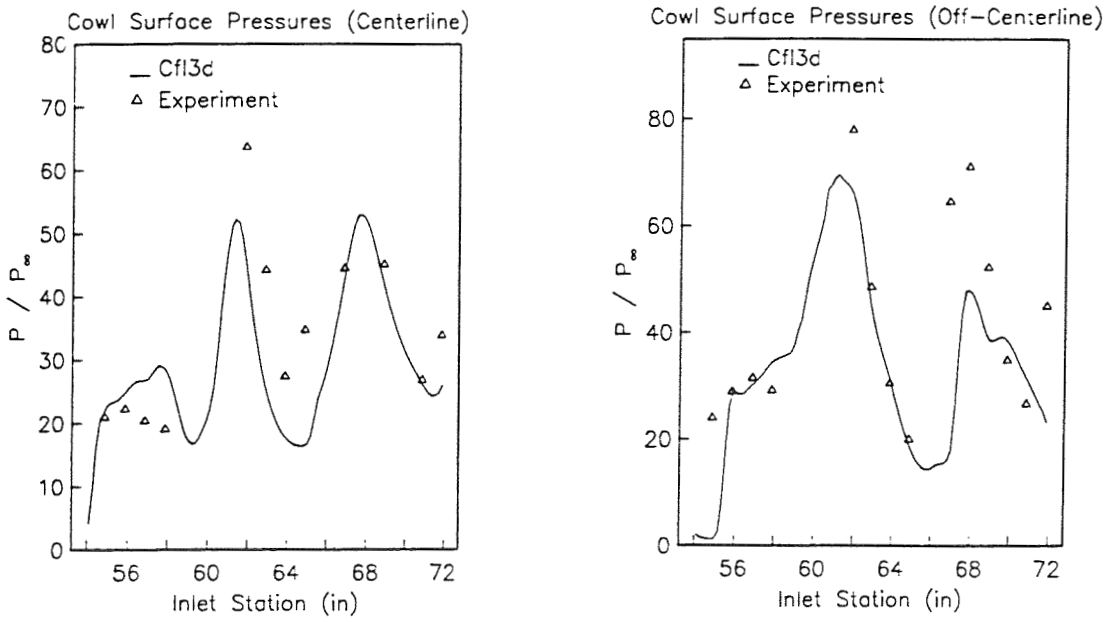

Figure 14. Pressure comparisons between CFL3D and experiment - 3-D Model, cowl surface centerline and off-centerline, inside inlet.

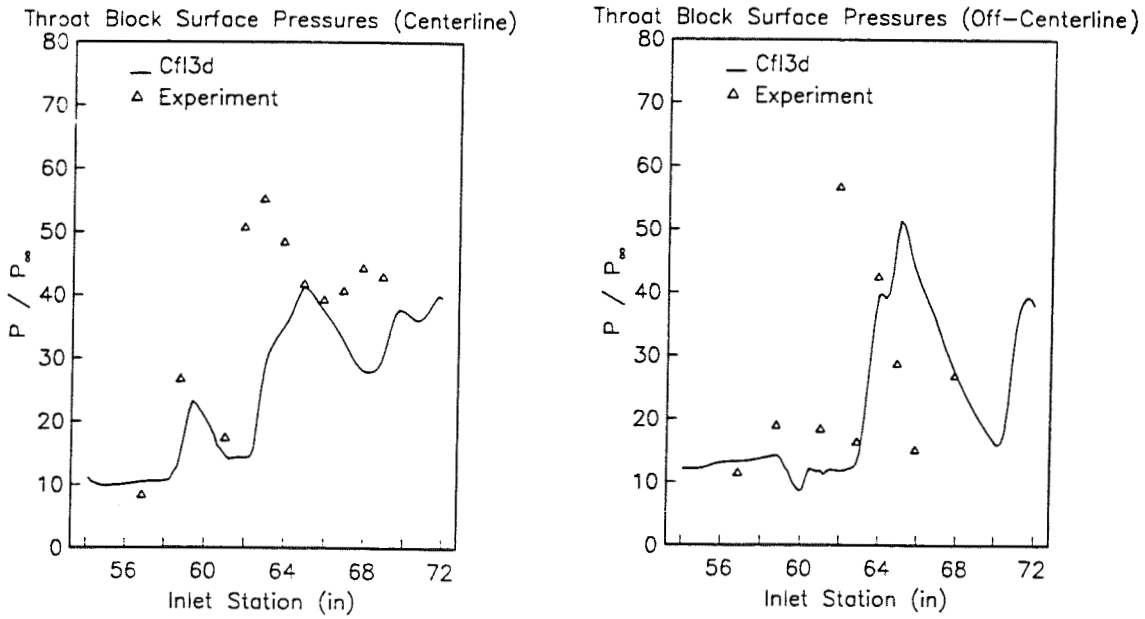

Figure 15. Pressure comparisons between CFL3D and experiment - 3-D Model, throat block surface centerline and off-centerline, inside inlet.

CONCLUSIONS

Using a zonal technique, computational results for two high-speed inlet flows have been obtained and compared with experimental data as part of a code validation study. The ability of the zonal version of CFL3D to supply reasonably accurate flow predictions for simple high-speed inlets is demonstrated by the 2-D Internal Flow Model results. These results indicate the importance of adequate grid refinement in calculating internal flows with shocks. The fine grid results exhibit better agreement with the peak values of the experimental heat transfer and pressure, and have reasonably good agreement overall with the experimental data. However, the agreement for the 3-D Forebody/Inlet Integration Model is not as good for the flow in the inlet. A more refined grid solution for this geometry is currently underway. Based on the 2-D Internal Flow Model results, grid refinement should improve the agreement with the experimental data and demonstrate the forebody/inlet capabilities of the zonal version of CFL3D.

REFERENCES

1. Vatsa, V. N.; Thomas, J. L.; and Wedan, B. W., "Navier-Stokes Computations of Prolate Spheroids at Angle of Attack," AIAA Paper 87-2627-CP (1987).

2. Richardson, P. F.; Parlette, E. B.; Morrison, J. H.; Switzer, G. F.; Dilley, A. D.; and Eppard, W. M., "Heat Transfer and Pressure Comparisons Between Computation and Wind Tunnel For a Research Hypersonic Aircraft," AIAA Paper 89-0029 (1989).

3. Rudy, D. H.; Kumar, A.; Thomas, J. L.; Gnoffo, P. A.; and Chakravarthy, S. U., "A Comparative Study and Validation of Upwind and Central-Difference Navier-Stokes Codes For High Speed Flows," In *Validation of Computational Fluid Dynamics*, AGARD-CP-437, Vol. 1, pp 37-1 to 37-15 (1988).

4. Thomas, J. L.; Rudy, D. H.; Chakravarthy, S. U.; and Walters, R. W., "Patched-Grid Computations of High-Speed Inlet Flows," In *Advances and Applications in Computational Fluid Dynamics*, A.S.M.E., FED-Vol. 66, pp. 11-22 (1988).

5. Rudy, D. H.; Thomas, J. L.; Kumar, A.; Gnoffo, P. A.; and Chakravarthy, S. U., "A Validation Study of Four Navier-Stokes Codes For High Speed Flows," AIAA Paper 89-1838 (1989).

6. "National Aerospace Plane Generic Option #2 Experimental Database/CFD Code Validation," McDonnell Douglas Corporation, Contract F33657-86-C-2126, September 1988.

7. Eriksson, L. E., "Practical Three-Dimensional Mesh Generation Using Transfinite Interpolation," In *SIAM Journal of Science and Statistical Computations*, July 1985, Vol. 6 no. 3, pp 712-741 (1985).

8. Baldwin, B. S. and Lomax, H., "Thin-Layer Approximation and Algebraic Model For Separated Turbulent Flows," AIAA Paper 78-257 (1987).

9. Reddy, D. R.; Smith, G. E.; Liou, M. F.; and Benson, T. J., "Three-Dimensional Viscous Analysis of a Hypersonic Inlet," AIAA Paper 89-0004 (1989).